

## Specific heat of matter formed in relativistic nuclear collisions

Sumit Basu, Sandeep Chatterjee, Rupa Chatterjee, and Tapan K. Nayak  
*Variable Energy Cyclotron Centre, Kolkata 700064, India*

Basanta K. Nandi

*Indian Institute of Technology Bombay, Mumbai 400076, India*

(Received 21 January 2016; published 3 October 2016)

We report the excitation energy dependence of specific heat ( $c_v$ ) of hadronic matter at freeze-out in Au+Au and Cu+Cu collisions at the BNL Relativistic Heavy Ion Collider energies by analyzing the published data on event-by-event mean transverse momentum ( $\langle p_T \rangle$ ) distributions. The  $\langle p_T \rangle$  distributions in finite  $p_T$  ranges are converted to distributions of effective temperatures, and dynamical fluctuations in temperature are extracted by subtracting widths of the corresponding mixed event distributions. The heat capacity per particle at the kinetic freeze-out surface is presented as a function of collision energy, which shows a sharp rise in  $c_v$  below  $\sqrt{s_{NN}} = 62.4$  GeV. We employ the hadron resonance gas (HRG) model to estimate  $c_v$  at the chemical and kinetic freeze-out surfaces. The experimental results are compared to the HRG and other theoretical model calculations. HRG results show good agreement with data. Model predictions for  $c_v$  at the CERN Large Hadron Collider energy are presented.

DOI: [10.1103/PhysRevC.94.044901](https://doi.org/10.1103/PhysRevC.94.044901)

### I. INTRODUCTION

The major goal of colliding heavy-ions at the Relativistic Heavy Ion Collider (RHIC) at Brookhaven National Laboratory and the Large Hadron Collider (LHC) at CERN is to study matter at extreme conditions of temperature and energy densities, where quarks and gluons, rather than mesons and baryons, define the relevant degrees of freedom [1]. This new phase of matter, the quark-gluon plasma (QGP), is governed by the principles of quantum chromodynamics (QCD) and is the result of a phase transition from the normal nuclear matter [2,3]. Experiments at RHIC and LHC are on the quest to unearth the nature of the QCD phase transition and to get a glimpse of how matter behaves at extreme conditions. The beam energy scan (BES) program at RHIC has been initiated to explore the onset of phase transition by scanning the collision energy over a larger range and to locate the critical point in the QCD phase diagram.

The thermodynamic state of the QCD matter can be specified by the temperature  $T$  and the chemical potentials  $\mu_B$ ,  $\mu_S$ , and  $\mu_Q$  corresponding to the conserved charges of QCD, namely baryon number ( $B$ ), strangeness ( $S$ ), and electric charge ( $Q$ ), respectively. Phase transitions are associated with the transformation of thermodynamic quantities such as pressure, entropy, and energy density, as well as a set of response functions, like, specific heat, compressibility, and susceptibility with change in  $T$ ,  $\mu_B$ ,  $\mu_Q$ , and  $\mu_S$ . In this article, we discuss the specific heat ( $c_v$ ) of the system produced in heavy-ion collisions at relativistic energies and its behavior as a function of collision energy.

Specific heat is a thermodynamic quantity characterizing the equation of state of the system. For a system undergoing phase transition,  $c_v$  is expected to diverge at the critical point. Temperature fluctuation of the system provides an estimation of  $c_v$ . Near the critical point, the specific heat is normally expressed in terms of a power law,  $c_v \propto |T - T_c|^{-\alpha}$ , where

$T_c$  is the critical temperature and  $\alpha$  is critical exponent. Thus the variation of thermal fluctuations with temperature can be effectively used to probe the critical point.

Hadron resonance gas (HRG) model analysis of the particle yields indicate the formation of a thermal source for the produced particles in heavy-ion collisions [4,5]. The production of a large number of particles in each collision at the RHIC and LHC energies makes it even possible to study several quantities on an event-by-event basis [4–9] and hence measure their event to event fluctuations. Thus, with the measurement of  $T$  on an event-by-event basis, it is possible to extract the  $c_v$  of the hot and dense strongly interacting matter produced in heavy-ion collisions. Assuming complete thermal equilibrium up to the surface of last scattering which is the kinetic freeze-out surface,  $c_v$  is then expected to reveal the thermodynamic state of the matter at the moment of kinetic freeze-out.

The specific heat and its variation as a function of temperature have been studied extensively in different theoretical calculations. Statistical and HRG models have been used to obtain  $c_v$  as a function of temperature in hadron gas and in quark-gluon matter [10–13]. In Ref. [11], a parton and hadron cascade model has been used to investigate  $c_v$  as a function of beam energy for the initial partonic stage using quark-gluon matter and the final stage using hadronic matter. Lattice QCD calculations [14–16] provide estimations of  $c_v$  for a wide range of temperatures. In Ref. [14], continuum limits of  $c_v$  have been calculated in quenched QCD at temperatures of  $2T_c$  and  $3T_c$ , where  $T_c$  is the transition temperature. It is found that  $c_v$  differs significantly from that of the ideal gas. Recent lattice calculations using (2+1)-flavor QCD with almost physical quark masses give the results of  $c_v$  for a temperature range of 130 to 400 MeV [15]. The low temperature (hadron phase) results agree well with HRG.

The specific heat has its origin in the event-by-event temperature fluctuations, which manifests through the fluctuations in the transverse momenta ( $p_T$ ) [4,5,11–13,17–21].

Event-by-event fluctuations of  $\langle p_T \rangle$  have been reported by experiments at the CERN Super Proton Synchrotron (SPS) [22–25] and beam energy scan at RHIC [26–29]. The values of  $c_v$  extracted from the experimental results have large errors [21,23,24,30]. The  $p_T$  fluctuation data from Ref. [22] yielded the value of  $c_v$  to be  $60 \pm 100$  at  $T = 180$  MeV for SPS energies. The statistical fluctuations arising from the finite multiplicity distributions of charged particles may significantly affect the extracted thermodynamic fluctuations [17]. In the present work, this is taken care of by subtracting the widths of the results of mixed events from the real data. Since radial flow affects the estimation of temperature, its effect has also been considered. Finally, the values of  $c_v$  have been calculated as a function of beam energy from published experimental data and compared to lattice and HRG calculations. Further predictions have been made for the LHC energies.

The paper is organized as follows. In Sec. II, we present the methodology for extraction of  $c_v$  from event-by-event average transverse momentum distributions and from theoretical calculations. The HRG model calculations of specific heat are presented in Sec. III. Event-by-event distributions of mean transverse momenta have been reported by several experiments at CERN-SPS and RHIC. The  $\langle p_T \rangle$  distributions and corresponding values of effective temperatures are presented in Sec. IV. A compilation of the results of specific heat from the existing experimental data is presented in Sec. V. Estimates for the specific heat at LHC using the AMPT model [32] have been included in this section. A discussion on the results of  $c_v$  is given in Sec. VI. The paper is summarized with an outlook in Sec. VII.

## II. SPECIFIC HEAT: METHODOLOGY

The heat capacity  $C$  of a system is defined as [37]

$$C = \left( \frac{\partial E}{\partial T} \right)_V, \quad (1)$$

where  $T$ ,  $V$ , and  $E$  are temperature, volume, and energy of the system, respectively. Equivalently,  $C$  of a system in thermal equilibrium to a bath at  $T$  can be computed from the event-by-event fluctuations of  $E$ :

$$C = \frac{\langle (E^2) \rangle - \langle E \rangle^2}{\langle T \rangle^2}. \quad (2)$$

For a system in equilibrium, the event-by-event temperature fluctuation is controlled by the heat capacity:

$$P(T) \sim \exp \left[ -\frac{C}{2} \frac{(\Delta T)^2}{\langle T \rangle^2} \right], \quad (3)$$

where  $\langle T \rangle$  is the mean temperature and  $\Delta T = T - \langle T \rangle$  is the variance in temperature. This yields the expression for  $C$  [4–6,11,37]:

$$\frac{1}{C} = \frac{\langle (T^2) \rangle - \langle T \rangle^2}{\langle T \rangle^2}. \quad (4)$$

Heat capacity thus can be estimated from the fluctuations in energy or temperature. For a system in equilibrium, the mean values of  $T$  and  $E$  are related by an equation of state. However, the fluctuations in energy and temperature have very different

behavior. Energy being an extensive quantity, its fluctuation has a volume dependent component. So energy is not suited for obtaining the heat capacity. On the other hand, temperature fluctuations provide a good major for estimating the  $c_v$  [4–6,37].

The temperature of the system can be obtained from the transverse momentum ( $p_T$ ) spectra of the emitted particles. An exponential Boltzmann-type fit to the  $p_T$  spectra gives a measure of the temperature:

$$F(p_T) = \frac{1}{p_T} \frac{dN}{dp_T} \approx A e^{-p_T/T_{\text{eff}}}, \quad (5)$$

where  $A$  is a normalization factor and  $T_{\text{eff}}$  is the apparent or effective temperature of the system [11]. For obtaining the event-by-event fluctuation, the temperature needs to be estimated in every event. The fitting is possible only for central heavy-ion collisions at the LHC energies when the number of particles is at least one thousand in every event. Even in this case, the error associated with the fitting will be relatively large. This can be overcome by making a connection of mean transverse momentum ( $\langle p_T \rangle$ ) of particles in every event with the temperature. Since the calculation of the mean value is more stable, this method of temperature estimation can also be used for collisions at RHIC energies. The  $\langle p_T \rangle$  can be written as [29]

$$\langle p_T \rangle = \frac{\int_0^\infty p_T^2 F(p_T) dp_T}{\int_0^\infty p_T F(p_T) dp_T} \quad (6)$$

$$= \frac{2T_{\text{eff}}^2 + 2m_0 T_{\text{eff}} + m_0^2}{m_0 + T_{\text{eff}}}, \quad (7)$$

where  $m_0$  is the rest mass of the particle. Note that the integration for  $p_T$  is from 0 to  $\infty$ . But in reality the  $p_T$  window is finite. For a range of  $p_T$  within  $a$  to  $b$ , we obtain

$$\langle p_T \rangle = \frac{\int_a^b p_T^2 F(p_T) dp_T}{\int_a^b p_T F(p_T) dp_T} \quad (8)$$

$$= 2T_{\text{eff}} \quad (9)$$

$$+ \frac{a^2 e^{-a/T_{\text{eff}}} - b^2 e^{-b/T_{\text{eff}}}}{(a + T_{\text{eff}})e^{-a/T_{\text{eff}}} - (b + T_{\text{eff}})e^{-b/T_{\text{eff}}}}. \quad (10)$$

This equation links the value of  $\langle p_T \rangle$  within a specified range of  $p_T$  to  $T_{\text{eff}}$ .

In order to validate the relation between  $p_T$  to  $T_{\text{eff}}$ , we have generated a large number of events using the AMPT model [32] for Pb+Pb collisions at  $\sqrt{s_{NN}} = 2.76$  TeV. The goal is to compare the values of  $T_{\text{eff}}$  obtained from event-by-event  $p_T$  distribution and from  $\langle p_T \rangle$  distributions. For top central (top 5% cross section) collisions,  $p_T$  distribution of pions has been constructed for each event within a rapidity range of  $-1.0$  to  $1.0$ . The distribution is fitted to an exponential function and the inverse slope parameter ( $T_{\text{eff}}$ ) is extracted within fit range,  $0.15 < p_T < 2.0$  GeV. Figure 1 shows the extracted event-by-event  $T_{\text{eff}}$  distribution (as solid circles). For the same set of events, the values of  $\langle p_T \rangle$  has been calculated within the same  $\eta$  and  $p_T$  ranges for each event. From the value of  $\langle p_T \rangle$  for each event, the  $T_{\text{eff}}$  is calculated using Eq. (10). The resulting  $T_{\text{eff}}$  distribution has been plotted as open squares in

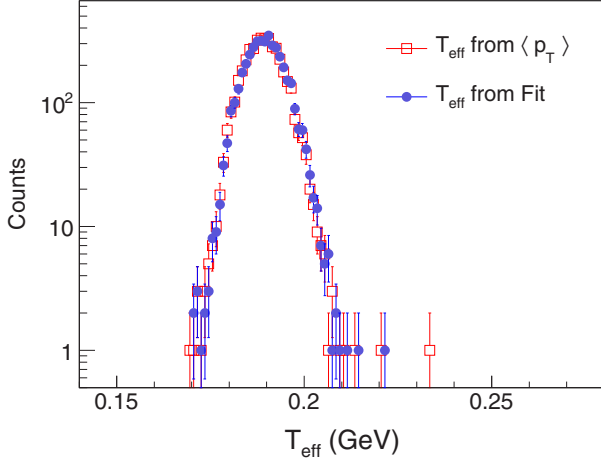


FIG. 1. Event-by-event  $T_{\text{eff}}$  distributions of pions for central Pb+Pb collisions at  $\sqrt{s_{NN}} = 2.76$  TeV from the AMPT model within rapidity range of  $-1.0$  to  $1.0$  and  $0.15 < p_T < 2.0$  GeV.  $T_{\text{eff}}$  distributions, obtained by fitting the  $p_T$  distribution of each event and from the  $\langle p_T \rangle$  are presented.

Fig. 1. Both the  $T_{\text{eff}}$  distributions are observed to be same. This validates the relationship of  $\langle p_T \rangle$  and  $T_{\text{eff}}$  as given in Eq. (10).

We note that the extracted temperature,  $T_{\text{eff}}$ , is a combination of kinetic freeze-out temperature ( $T_{\text{kin}}$ ) and transverse flow velocity ( $\beta_T$ ) of the system:

$$T_{\text{eff}} = T_{\text{kin}} + f(\beta_T). \quad (11)$$

For pion,  $f(\beta_T) \approx m_0 \langle \beta_T \rangle^2$ . The event-by-event fluctuations of  $\beta_T$  needs to be taken into account for calculating the fluctuation in kinetic temperature [19,38–40]. Fluctuation in  $\beta_T$  dominates over the fluctuation in  $T_{\text{kin}}$  for small systems (e.g.,  $pp$ ) [41], asymmetric (e.g.,  $p$  Pb) [19] and noncentral collisions. For central Au+Au collisions at  $\sqrt{s_{NN}} = 200$  GeV [44],  $\beta_T = 0.59 \pm 0.051$  and for central Pb+Pb collisions at  $\sqrt{s_{NN}} = 2.76$  TeV [45],  $\beta_T = 0.651 \pm 0.02$ , which translate to  $T_{\text{kin}}$  as  $0.095 \pm 0.010$  GeV and  $0.09 \pm 0.005$  GeV, respectively by using blast-wave fit [42]. For the present work, we consider 10% fluctuation in  $\beta_T$  and calculate its effect on specific heat.  $C$  is calculated using the equation

$$\begin{aligned} \frac{1}{C} &= \frac{(\langle T_{\text{kin}}^2 \rangle - \langle T_{\text{kin}} \rangle^2)}{\langle T_{\text{kin}} \rangle^2} \approx \frac{(\langle T_{\text{eff}}^2 \rangle - \langle T_{\text{eff}} \rangle^2)}{\langle T_{\text{kin}} \rangle^2} \\ &= \frac{(\Delta T_{\text{eff}})^2}{\langle T_{\text{kin}} \rangle^2}. \end{aligned} \quad (12)$$

The values of  $\langle T_{\text{kin}} \rangle$  are obtained from the blast-wave fits to the  $p_T$  distributions of identified particles. With this, we obtain the specific heat as the heat capacity per number of particles ( $N$ ) as ( $c_v = C/N$ ) within the system.

Let us put the specific heat calculated in the present scenario (heat capacity per particle) in perspective with quantities normally quoted in theoretical calculations. For an ideal gas of particles of mass  $m$  and degeneracy factor  $g$  at temperature  $T$ , zero chemical potential, and volume  $V$ , the number of particles

$N(T, V)$  can be expressed using Boltzmann statistics:

$$\begin{aligned} N &= g \int \frac{d^3x d^3p}{h^3} \exp \left[ -\frac{\sqrt{p^2 + m^2}}{T} \right] \\ &= g \int d^3x \int \frac{d^3p}{h^3} \exp \left[ -\frac{\sqrt{p^2 + m^2}}{T} \right] \\ &= g \frac{VT^3}{(2\pi)^3} \int d^3q \exp[-\sqrt{q^2 + (m/T)^2}] \\ &= g \frac{VT^3}{(2\pi)^3} \alpha, \end{aligned} \quad (13)$$

where  $q = p/T$ ,  $\alpha = \int d^3q \exp[-\sqrt{q^2 + (m/T)^2}]$ , and we have taken  $\hbar = h/(2\pi) = 1$ . The energy  $E(T, V)$  is given by

$$E = g \int \frac{d^3x d^3p}{h^3} \sqrt{p^2 + m^2} \exp \left[ -\frac{\sqrt{p^2 + m^2}}{T} \right]. \quad (14)$$

The heat capacity [from Eq. (1)] can be written as

$$\begin{aligned} C &= g \int d^3x \int \frac{d^3p}{h^3} \left( \frac{p^2 + m^2}{T^2} \right) \exp \left[ -\frac{\sqrt{p^2 + m^2}}{T} \right] \\ &= g \frac{VT^3}{(2\pi)^3} \int d^3q \left( q^2 + \left( \frac{m}{T} \right)^2 \right) \exp \left[ -\sqrt{q^2 + \left( \frac{m}{T} \right)^2} \right] \\ &= g \frac{VT^3}{(2\pi)^3} \beta. \end{aligned} \quad (15)$$

$\beta = \int d^3q \left( q^2 + \left( \frac{m}{T} \right)^2 \right) \exp[-\sqrt{q^2 + (m/T)^2}]$  is a dimensionless quantity. The specific heat is the heat capacity per unit phase space volume,

$$c_v = C/\Delta, \quad (16)$$

where  $\Delta$  is an estimate of the phase space volume. In lattice calculations one extracts the dimensionless quantity  $C/(VT^3)$  and investigate its temperature dependence [15], so in these calculations  $\Delta = VT^3$ . However, in experiments it is simpler to measure the dimensionless quantity  $C/N$ , where  $N$  is the charged particle multiplicity, and thus  $\Delta = N$ , where  $N$  is taken as pseudorapidity ( $\eta$ ) density of charged particles at midrapidity ( $dN_{\text{ch}}/d\eta$  at  $\eta = 0$ ). We compare the experimental results to other model calculations for  $C/N$  as in Ref. [11], where a parton and hadron cascade model, PACIAE has been used to compute  $C/N$ . We also compare with HRG where it is straightforward to obtain both  $C/(VT^3)$  and  $C/N$ .

### III. HADRON RESONANCE GAS MODEL AND SPECIFIC HEAT

The current continuum estimates of lattice QCD thermodynamics in the low temperature and density phase (hadronic phase) show good agreement with that of an ideal hadron resonance gas [33–35]. Assuming complete chemical equilibrium between all hadrons, the hadron chemical potential of the  $i$ th species  $\mu_i$  can be written as

$$\mu_i = B_i \mu_B + Q_i \mu_Q + S_i \mu_S, \quad (17)$$

where  $B_i$ ,  $Q_i$ , and  $S_i$  are the baryon number, electric charge, and strangeness quantum numbers of the  $i$ th hadron, respectively. The HRG partition function  $Z$  in the grand canonical ensemble at  $(T, \mu_B, \mu_S, \mu_Q)$  can be expressed as

$$\ln Z = VT^3 \sum_i \frac{g_i}{2\pi^2} \left(\frac{m_i}{T}\right)^2 \sum_{l=1}^{\infty} (-a)^{l+1} l^{-2} K_2(lm_i/T) \times \exp[l(B_i\mu_B + Q_i\mu_Q + S_i\mu_S)/T], \quad (18)$$

where the sum runs over all hadrons and resonances up to mass  $\sim 2$  GeV as listed in the Review of Particle Physics [36].  $a = -1$  for mesons and 1 for baryons. Here  $g_i$ ,  $m_i$ ,  $B_i$ ,  $Q_i$ , and  $S_i$  refer to the properties of the  $i$ th hadron species: its degeneracy factor, mass, baryon number, electric charge, and strangeness, respectively.  $V$  is the volume of the fireball under study.  $K_2$  is the modified Bessel function of the second kind. From  $\ln Z$ , all thermodynamic quantities could be computed.

From  $\ln Z$ ,  $E$  is obtained as follows:

$$E = T^2 \frac{\partial \ln Z}{\partial T} + \sum_i \mu_i N_i, \quad (19)$$

where

$$N_i = T \frac{\partial \ln Z}{\partial \mu_i}. \quad (20)$$

From  $E$  it is straightforward to compute  $C$  using Eq. (1).

The values of  $T_{\text{kin}}$  have been reported by experiments at RHIC and LHC, as the final state particles give the information about  $T_{\text{kin}}$  from the particle spectra [43]. These are obtained by making combined fits to the identified particle spectra using the Boltzmann-Gibbs blast-wave model. Figure 2 gives the  $T_{\text{kin}}$  values for different beam energies and collision systems [29,44,45]. In addition, chemical freeze-out temperatures ( $T_{\text{ch}}$ ), extracted from the identified particle yield by using thermal model calculations [46,47], are also shown in the figure. We find that the difference between  $T_{\text{ch}}$  and  $T_{\text{kin}}$

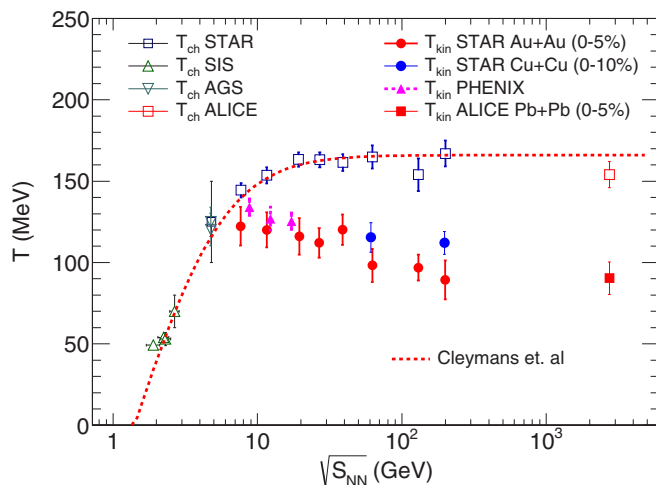


FIG. 2. Chemical and kinetic freeze-out temperatures for central Au+Au [44] and Cu+Cu [29] collisions at RHIC energies, and Pb+Pb collisions at  $\sqrt{s_{NN}} = 2.76$  TeV [45]. Thermal model calculation [46] to  $T_{\text{ch}}$  is also shown.

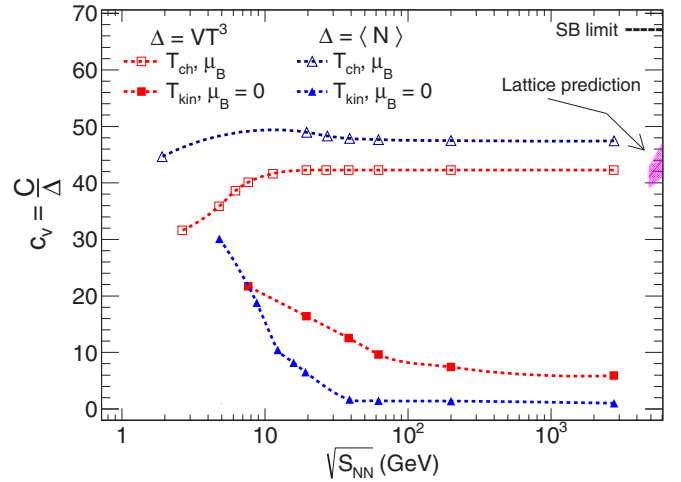


FIG. 3. Specific heat,  $c_v$  as a function of collision energy from the HRG model for two temperature settings,  $T_{\text{ch}}$  with finite  $\mu_B$ , and  $T_{\text{kin}}$ , and two phase space volumes,  $\Delta = VT^3$  and  $\langle N \rangle$ . Lattice calculation for  $c_v$  at  $T = 154 \pm 9$  MeV [15] and Stefan-Boltzmann limit are indicated in the figure.

increases with the increase of beam energy. Lattice calculations indicate that  $c_v$  is a monotonically increasing function of  $T$  at zero  $\mu_B$ . Thus we expect that the difference between the  $c_v$  extracted at the chemical and kinetic freeze-out surfaces should also increase with beam energy following the trends of  $T_{\text{ch}}$  and  $T_{\text{kin}}$ .

We calculate  $c_v$  from HRG model for two scenarios. In the first case, we compute at the chemical freeze-out surface using the extracted  $T_{\text{ch}}$  as well as  $\mu_B$ . However, in the experiment one can only determine the  $c_v$  at the kinetic freeze-out surface where the momentum exchange freezes. The thermal conditions at the kinetic freeze-out surface are much different from that at the chemical freeze-out surface. Hence the fireball is expected to have different  $c_v$  at the two surfaces. In the second case, we try to estimate  $c_v$  at the kinetic freeze-out surface using  $T_{\text{kin}}$  and zero hadron chemical potentials. For both scenarios, we calculate  $C/(VT^3)$  and  $C/N$  for a wide range of beam energy, from  $\sqrt{s_{NN}} = 1.91$  GeV to 2.76 TeV. The results of  $c_v$  are shown in the Fig. 3. It is observed that the trend of  $c_v$  as a function of  $\sqrt{s_{NN}}$  is similar to the nature followed by chemical and kinetic freeze-out temperatures. The value of  $C/N$  corresponding to  $T_{\text{kin}}$  shows a sharp drop with increase of energy, and beyond  $\sqrt{s_{NN}} = 62.4$  GeV, the rate of decrease is very slow. A better estimate of  $c_v$  in HRG could be made with realistic hadron chemical potentials taking into account the conservation of hadron number from the chemical to the kinetic freeze-out surfaces.

Recent lattice calculations for  $c_v$  have been reported [15] as a function of temperature. The lattice results are at zero baryonic potential, hence only relevant at the LHC and higher energies. The value of  $c_v$  as indicated in the Fig. 3 is for  $T = 154 \pm 9$  MeV, corresponding to the QCD transition temperature. It is seen that at the transition temperature and below, HRG results of  $C/(VT^3)$  agree well with lattice calculations [15]. The Stefan-Boltzmann noninteracting gas limit ( $c_v \approx 66$ ) is also shown in the figure.

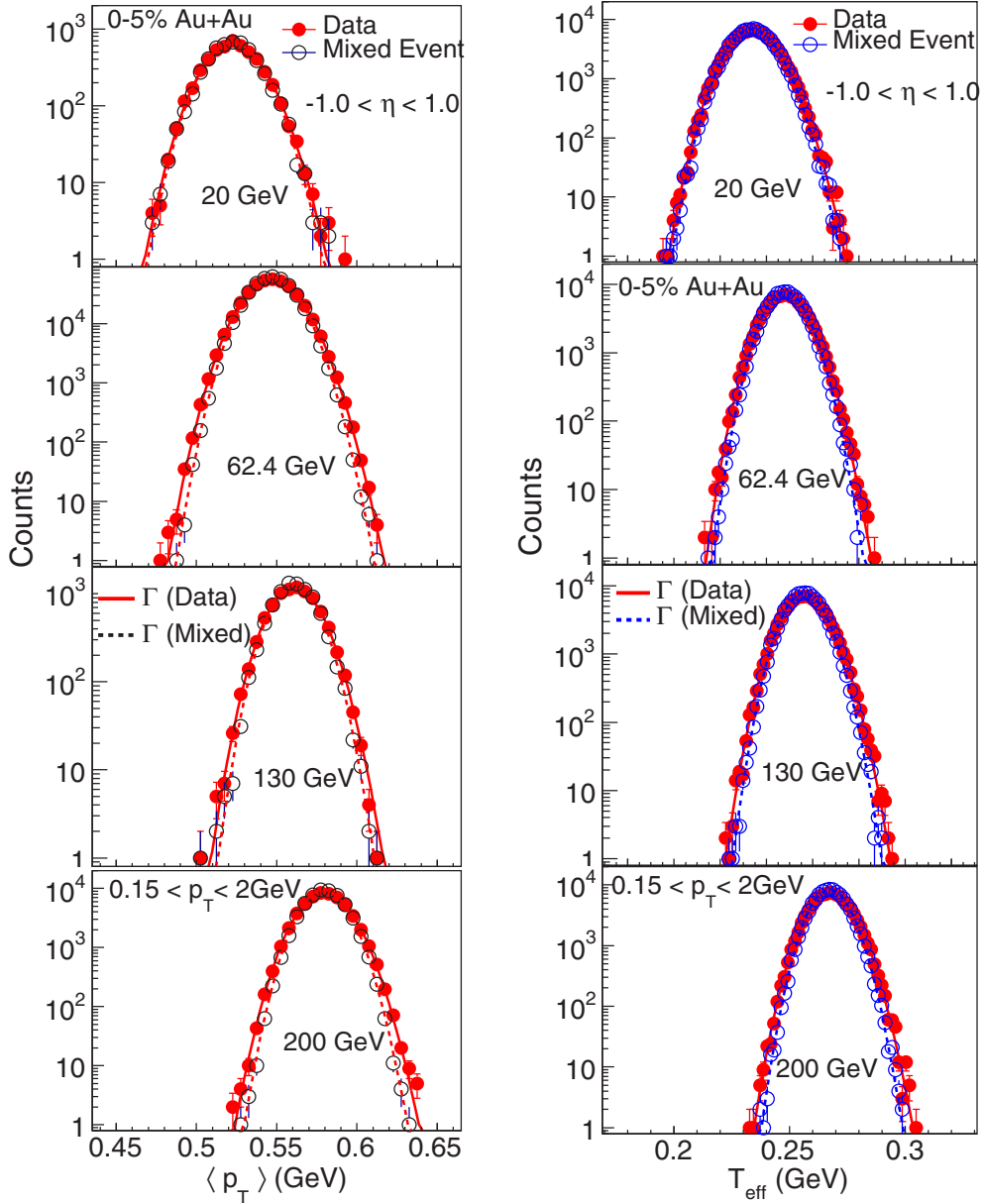


FIG. 4. Left panels show event-by-event mean transverse momentum distributions for 5% most central Au+Au collisions at  $\sqrt{s_{NN}} = 20, 62.4, 130,$  and  $200$  GeV within  $|\eta| < 1$  and  $0.15 < p_T < 2.0$  GeV [28]. Distributions for mixed events are superimposed on the data. The solid and dashed lines show the fits with  $\Gamma$  functions. The right panels show the extracted  $T_{\text{eff}}$  distributions for each incident energy.

#### IV. DISTRIBUTIONS OF $\langle p_T \rangle$ AND $T_{\text{eff}}$

Experimental data for  $\langle p_T \rangle$  distributions have been reported by experiments at SPS and RHIC [22–28]. In the left panel of Fig. 4 we present the  $\langle p_T \rangle$  distributions from the STAR experiment [27,28] for the 5% most central Au+Au collisions at  $\sqrt{s_{NN}} = 20, 62.4, 130,$  and  $200$  GeV. The results are shown for charged particle tracks within  $|\eta| < 1$  and  $0.15 < p_T < 2.0$  GeV. The solid points are the event-by-event  $\langle p_T \rangle$  distributions from the experimental data, whereas the open circles are the corresponding results for mixed events. The mixed events are created by randomly selecting charged particles from different events. The mixed event distributions contain all the systematic effects arising from the detector effects,

such as efficiency and acceptance, as well as include statistical fluctuations. The nonstatistical or dynamical fluctuations in  $\langle p_T \rangle$  can be extracted by subtracting the width of the mixed event distribution from that of the real data.

It has been observed that the  $\langle p_T \rangle$  distributions are nicely described by using the gamma ( $\Gamma$ ) distribution [27,28,31]:

$$f(x) = \frac{x^{\alpha-1} e^{-x/\beta}}{\Gamma(\alpha)\beta^\alpha}. \quad (21)$$

Here  $x$  represents the  $\langle p_T \rangle$ . The mean ( $\mu$ ) and standard deviation ( $\sigma$ ) of the distribution are related to the fit parameters ( $\alpha$  and  $\beta$ ) by  $\mu = \alpha\beta$  and  $\sigma = \sqrt{\alpha\beta^2}$ . Both the real and mixed event  $\langle p_T \rangle$  distributions are fitted with the  $\Gamma$  function and the

TABLE I. The event-by-event  $T_{\text{eff}}$  distributions for central (top 5%) Au+Au collisions are fitted by the  $\Gamma$  function. Table gives the fit parameters,  $\alpha$  and  $\beta$  along with mean ( $\mu$ ) and standard deviation ( $\sigma$ ).

$\sqrt{s_{NN}}$ (GeV)	Case	$\alpha$	$\beta$ (GeV)	$\mu$ (GeV)	$\sigma$ (GeV)
20	data	658.53	$3.556 \times 10^{-4}$	0.2341	0.00912
20	mixed	724.56	$3.229 \times 10^{-4}$	0.2339	0.00869
62.4	data	860.20	$2.885 \times 10^{-4}$	0.2482	0.00846
62.4	mixed	1043.67	$2.378 \times 10^{-4}$	0.2481	0.00768
130	data	920.25	$2.789 \times 10^{-4}$	0.2566	0.00846
130	mixed	1140.12	$2.249 \times 10^{-4}$	0.2564	0.00759
200	data	1078.23	$2.483 \times 10^{-4}$	0.2677	0.00815
200	mixed	1387.56	$1.927 \times 10^{-4}$	0.2674	0.00718

fits are shown by the solid and dashed lines, respectively, in the left panels of Fig. 4. The fitted distributions are used to generate a large number of  $\langle p_T \rangle$  values for which corresponding  $T_{\text{eff}}$  values are calculated from Eq. (10). The resulting histograms represent event-by-event  $T_{\text{eff}}$  distributions, which are shown in the right panels of Fig. 4 for both real data and mixed events. These distributions are also fitted by the  $\Gamma$  function as shown by the solid and dashed lines for data and mixed events, respectively. Table I lists the fit parameters for event-by-event  $T_{\text{eff}}$  distributions for data and mixed events.

The system size dependence of  $\langle p_T \rangle$  and  $T_{\text{eff}}$  distributions have been studied with the STAR experimental data of top 10% central Cu+Cu collisions at  $\sqrt{s_{NN}} = 62.4$  and 200 GeV [29]. The results are presented in Fig. 5. Corresponding  $\Gamma$  distribution fit parameters to the event-by-event  $T_{\text{eff}}$  distributions for top 10% central collisions are tabulated in Table II.

TABLE II. The event-by-event  $T_{\text{eff}}$  distributions for central (top 10%) Cu+Cu collisions are fitted by the  $\Gamma$  function. Table gives the fit parameters,  $\alpha$  and  $\beta$  along with mean ( $\mu$ ) and standard deviation ( $\sigma$ ).

$\sqrt{s_{NN}}$ (GeV)	Case	$\alpha$	$\beta$ (GeV)	$\mu$ (GeV)	$\sigma$ (GeV)
62.4	data	211.88	$12.040 \times 10^{-4}$	0.2550	0.0175
62.4	mixed	271.94	$9.455 \times 10^{-4}$	0.2571	0.0156
200	data	277.08	$9.687 \times 10^{-4}$	0.2684	0.0161
200	mixed	370.71	$7.278 \times 10^{-4}$	0.2698	0.0140

From these two figures and the given tables for  $\langle p_T \rangle$  and  $T_{\text{eff}}$  distributions for Au+Au and Cu+Cu collisions at RHIC energies, we can infer that (a) the mean values of the event-by-event  $\langle p_T \rangle$  and  $T_{\text{eff}}$  consistently increase with the increase of beam energy, (b) the widths of the distributions decrease with the increase of beam energy. In addition, the widths for Cu+Cu system are observed to be larger compared to the corresponding widths of the Au+Au system. This may be because of the smaller system size for Cu+Cu compared to Au+Au system.

Experimental data for event-by-event  $\langle p_T \rangle$  distributions are not available for Pb+Pb collisions at LHC energies [48]. The string melting mode of AMPT model is used to generate central (top 5%) Pb+Pb collisions at  $\sqrt{s_{NN}} = 2.76$  TeV. The  $\langle p_T \rangle$  and  $T_{\text{eff}}$  distributions are constructed from these generated events as shown in Fig. 1. This distribution will be used to extract specific heat at the LHC energy.

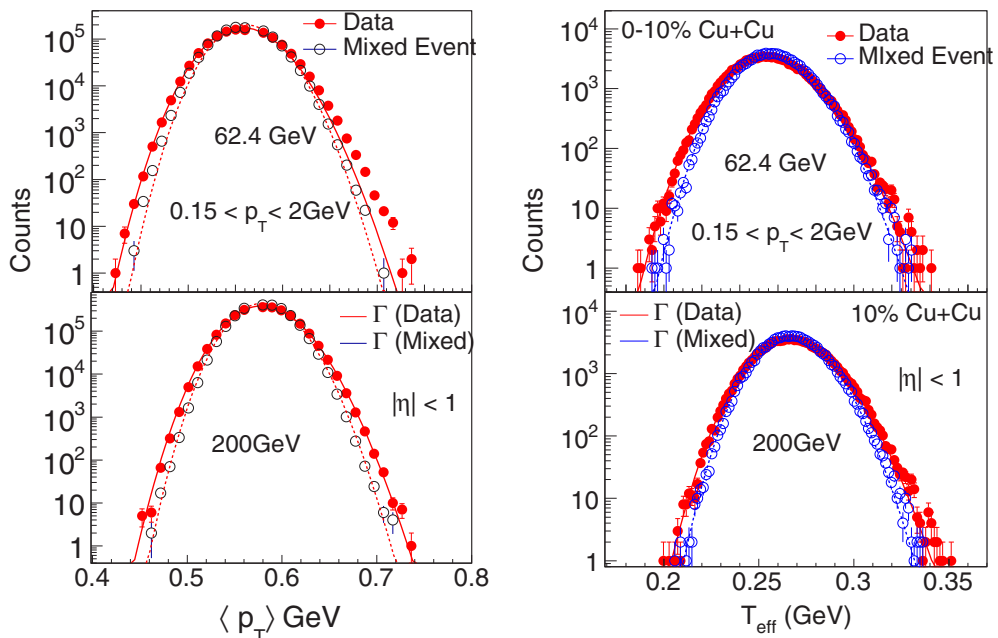


FIG. 5. Similar distributions as in Fig. 4 for 10% most central Cu+Cu collisions at  $\sqrt{s_{NN}} = 62.4$  and 200 GeV [29].

## V. SPECIFIC HEAT FROM EXPERIMENTAL DATA

The widths of the  $T_{\text{eff}}$  distributions are strongly affected by statistical fluctuations, which need to be subtracted as the heat capacity is related only to the dynamical part of the fluctuation. The width contains two components:

$$(\Delta T_{\text{eff}})^2 = (\Delta T_{\text{eff}}^{\text{dyn}})^2 + (\Delta T_{\text{eff}}^{\text{stat}})^2. \quad (22)$$

$\Delta T_{\text{eff}}^{\text{dyn}}$  values are obtained by subtracting the widths of the  $T_{\text{eff}}$  distributions for mixed events from the real data. With this, Eq. (12) is expressed as

$$\frac{1}{C} = \frac{(\Delta T_{\text{eff}}^{\text{dyn}})^2}{\langle T_{\text{kin}} \rangle^2}. \quad (23)$$

The heat capacity  $C$  is calculated from Eq. (23) by using the values of  $T_{\text{kin}}$  from Fig. 2. Knowing the heat capacity, the specific heat,  $c_v$  is obtained by dividing  $C$  by the number of charged particles in the system. Since the experimental results presented here are at midrapidity, we have divided the value of  $C$  by charged particle multiplicity at midrapidity [49,50] to obtain the specific heat. This is presented in Fig. 3 for Au+Au and Cu+Cu collisions at RHIC energies. The estimated  $C/N$  for the LHC energy from the AMPT model using Fig. 1 is also shown in the figure. The errors in the data points are estimated mainly from the following sources: (a) error in extraction of  $T_{\text{kin}}$  using the blast-wave fits, (b) error in charge particle multiplicity density, and (c) error in  $\langle p_T \rangle$  as reported in the experimental data. The error in  $T_{\text{kin}}$  takes into account the spread in the value of  $\langle \beta_T \rangle$ . It is observed that  $C/N$  has a sharp drop from  $\sqrt{s_{NN}} = 20$  GeV to 62.4 GeV, beyond which the decrease is rather slow up to the LHC energy.

HRG calculations for  $C/N$  with  $T_{\text{kin}}$  are superimposed in Fig. 6. These results follow the experimental data points quite well. In Ref. [11], specific heat for central (top 5%) Au+Au collisions at RHIC energies are discussed using a parton and

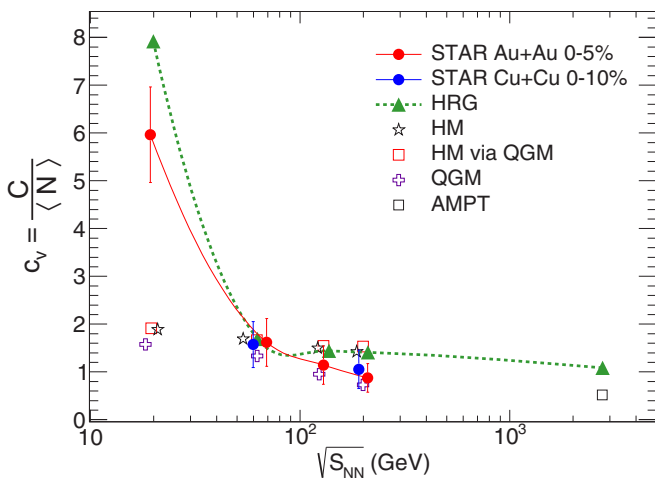


FIG. 6. Specific heat,  $c_v$  as a function of collision energy for central Au+Au and Cu+Cu collisions at RHIC energies. Result from AMPT model is given for the LHC energy at  $\sqrt{s_{NN}} = 2.76$  TeV. HRG calculations at  $T_{\text{kin}}$  are shown in the figure. Model calculations for three different scenarios from Ref. [11] are superimposed on the experimental results.

hadron cascade model, called PACIAE. The results of the model calculations are presented for three cases: hadronic matter (HM) in the final state, quark-gluon matter in the partonic initial state (QGM), and hadronic matter via quark-gluon matter (HM via QGM). These results for Au+Au collisions are also presented in Fig. 6. The results of these models miss the experimental data point at  $\sqrt{s_{NN}} = 20$  GeV, but can explain the data at higher energies. The PACIAE is a transport model with LO pQCD cross sections considered between partons. It might be possible that at lower beam energies, the LO pQCD description is not appropriate.

## VI. DISCUSSION

In an earlier publication by Korus *et al.* (Ref. [21]), the experimental data of  $p_T$  correlations from the NA49 experiment [22–24] for Pb+Pb collision at laboratory energy of 158 GeV had used to calculate specific heat, which yielded a value of  $60 \pm 100$ . The large error bars of these results made the reported results insignificant. One of the possible reasons for the large errors is the low particle multiplicity which gives a significant hindrance to the calculation of dynamic temperature fluctuations [17]. At the SPS energies,  $\langle p_T \rangle$  distributions have been reported by NA49 collaboration for laboratory energies of 20, 30, 40, 80, and 158 GeV [22–24] and the CERES collaboration at 40, 80, and 158 GeV [25]. In both of the data sets, the  $\langle p_T \rangle$  distributions for real data and mixed event are indistinguishable. These are also prominent in the ratio plots of real and mixed events as shown in Ref. [25]. Thus the extraction of dynamic fluctuation in temperature and so the specific heat is not possible. In the present work, we have probed much higher energy collisions, where the charged particle multiplicities in each event are large, allowing for the extraction of the dynamical part of the temperature fluctuation by overcoming the statistical fluctuations.

The results of specific heat for Cu+Cu collisions are close to that of Au+Au collisions. This shows that although a large change of volume happens in going from Cu+Cu to Au+Au systems, the two systems are not very different thermodynamically.

Several sources of uncertainty may affect the extraction of specific heat. In the context of the results presented in Fig. 6, three sources of uncertainty, viz., effect of finite particle multiplicity, spread of  $T_{\text{kin}}$  from the fits of  $p_T$  distributions, and the radial flow fluctuations, have been discussed. Apart from these, it is worthwhile to point out some other uncertainties. Fluctuations in the impact parameter of the collision and thus the fluctuation in the number of participating nucleons gives an uncertainty to the event-by-event mean  $p_T$  distribution. The choice of narrow bins in centrality has been made to minimize this uncertainty. Another source of uncertainty may come from the choice of the  $p_T$  window. The lower bound of the  $p_T$  window needs to be chosen properly in order to reduce the final state effects such as resonance decay and hadronic scattering. Similarly, the upper limit on  $p_T$  needs to be chosen such that the effect from minijets and jets are minimized. Although it is implicit that radial flow fluctuations are minimum for central collisions because of inherent symmetry of the system, its detailed study can be

made using an event-by-event hydrodynamic model. These studies will help to pin down the errors of the results extracted in Fig. 6.

## VII. SUMMARY

We have studied the excitation energy dependence of specific heat of hadronic matter formed in heavy-ion collisions corresponding to RHIC and LHC energies. In the present work, dynamical component of the temperature fluctuation is calculated from  $\langle p_T \rangle$  distributions. From this, the specific heat is obtained as heat capacity per charge particle. We employ the HRG model to calculate heat capacity from the variation of energy of the system with temperature. Results of the HRG calculations are close to the data. With increase of collision energy,  $c_v$  shows a sharp drop from low energy till  $\sqrt{s_{NN}} = 62.4$  GeV, beyond which the rate of decrease is very slow. In this regard, we look forward to results of BES program of RHIC, where the collision energy and centrality dependences of  $c_v$  are expected to provide important signatures for the onset of the QGP phase transition. In order to probe the QCD critical point, we propose a finer scan of beam energies for the second phase of BES program (BES-II) from 7.7 GeV to 62.4 GeV. A sudden change in  $c_v$  is expected at a particular beam energy within this range. Studies of heat capacity at

high baryon density and lower temperatures accessible at Facility for Antiproton and Ion Research (FAIR) would be of high interest, unless it is critically challenged by statistical fluctuations. Predictions for  $c_v$  at the LHC at  $\sqrt{s_{NN}} = 2.76$  TeV are made using different models. It will be interesting to obtain  $c_v$  at the highest LHC energy of  $\sqrt{s_{NN}} = 5.02$  TeV in order to make a direct comparison to lattice calculations. In literature, it has been also proposed to calculate thermal conductivity from transverse energy ( $E_T$ ) fluctuations, which can be explored in future studies. The excitation energy dependence of  $c_v$  provides important information regarding the thermodynamic properties, such as, heat conductivity, speed of sound ( $c_s^2$ ), compressibility ( $k_T$ ), etc., which may reveal better understandings of the matter formed in relativistic nuclear collisions.

## ACKNOWLEDGMENTS

S.C. acknowledges ‘‘Centre for Nuclear Theory’’ [PIC XII-R&D-VEC-5.02.0500], Variable Energy Cyclotron Centre for support. This research used resources of the LHC grid computing center at the Variable Energy Cyclotron Centre, Kolkata. S.B. acknowledges intense constructive discussions with Alexander Philipp Kalweit, Roberto Preghnella, Prithwish Tribedy, Steffen Bass, and Michael Weber.

- 
- [1] Y. Aoki, G. Endrodi, Z. Fodor, S. D. Katz, and K. K. Szabo, *Nature* **443**, 675 (2006).
- [2] J. W. Harris and B. Muller, *Annu. Rev. Nucl. Part. Sci.* **46**, 71 (1996).
- [3] P. Braun-Munzinger and J. Stachel, *Nature* **448**, 302 (2007).
- [4] L. Stodolsky, *Phys. Rev. Lett.* **75**, 1044 (1995).
- [5] E. V. Shuryak, *Phys. Lett. B* **423**, 9 (1998).
- [6] M. A. Stephanov, K. Rajagopal, and E. V. Shuryak, *Phys. Rev. Lett.* **81**, 4816 (1998).
- [7] M. A. Stephanov, K. Rajagopal, and E. Shuryak, *Phys. Rev. D* **60**, 114028 (1999).
- [8] M. Stephanov, *Phys. Rev. D* **65**, 096008 (2002).
- [9] H. Heiselberg, *Phys. Rep.* **351**, 161 (2001).
- [10] S. Chatterjee, R. M. Godbole, and S. Gupta, *Phys. Rev. C* **81**, 044907 (2010).
- [11] B.-H. Sa, X.-M. Li, S.-Y. Hu, S.-P. Li, J. Feng, and D.-M. Zhou, *Phys. Rev. C* **75**, 054912 (2007).
- [12] X.-M. Li *et al.* *Int. J. Mod. Phys. E* **16**, 1906 (2007).
- [13] Aram Mekjian, *Phys. Rev. C* **73**, 014901 (2006).
- [14] R. V. Gavai, S. Gupta, and S. Mukherjee, *Phys. Rev. D* **71**, 074013 (2005).
- [15] A. Bazavov *et al.*, *Phys. Rev. D* **90**, 094503 (2014).
- [16] Yoshitaka Hatta and Kenji Fukushima, [arXiv:hep-ph/0311267](https://arxiv.org/abs/hep-ph/0311267).
- [17] S. A. Voloshin, V. Koch, and H. G. Ritter, *Phys. Rev. C* **60**, 024901 (1999).
- [18] W. Broniowski, B. Hiller, W. Florkowski, and P. Bozek, *Phys. Lett. B* **635**, 290 (2006).
- [19] P. Bozek and W. Broniowski, *Phys. Rev. C* **85**, 044910 (2012).
- [20] M. Bleicher *et al.*, *Nucl. Phys. A* **638**, 391c (1998).
- [21] R. Korus, S. Mrowczynski, M. Rybczynski, and Z. Wlodarczyk, *Phys. Rev. C* **64**, 054908 (2001).
- [22] H. Appelshauser (NA49 Collaboration), *Phys. Lett. B* **459**, 679 (1999).
- [23] T. Anticic (NA49 Collaboration), *Phys. Rev. C* **70**, 034902 (2004).
- [24] T. Anticic (NA49 Collaboration), *Phys. Rev. C* **79**, 044904 (2009).
- [25] D. Adamova (CERES Collaboration), *Nucl. Phys. A* **727**, 97 (2003).
- [26] K. Adcox (PHENIX Collaboration), *Phys. Rev. C* **66**, 024901 (2002).
- [27] J. Adams (STAR Collaboration), *Phys. Rev. C* **71**, 064906 (2005).
- [28] J. Adams (STAR Collaboration), *Phys. Rev. C* **72**, 044902 (2005).
- [29] L. Adamczyk (STAR Collaboration), *Phys. Rev. C* **87**, 064902 (2013).
- [30] M. J. Tannenbaum, [arXiv:nucl-ex/0512004](https://arxiv.org/abs/nucl-ex/0512004).
- [31] M. J. Tannenbaum, *Phys. Lett. B* **498**, 29 (2001).
- [32] Z.-W. Lin, C. M. Ko, B.-A. Li, B. Zhang, and S. Pal, *Phys. Rev. C* **72**, 064901 (2005).
- [33] A. Bazavov, T. Bhattacharya, M. Cheng *et al.*, *Phys. Rev. D* **80**, 014504 (2009).
- [34] S. Borsanyi, Z. Fodor, C. Hoelbling *et al.*, *J. High Energy Phys.* **09** (2010) 73.
- [35] S. Borsanyi, Z. Fodor, S. D. Katz, S. Krieg, C. Ratti, and K. Szabo, *J. High Energy Phys.* **2012**, 138 (2012).
- [36] K. A. Olive (Particle Data Group), *Chin. Phys. C* **38**, 090001 (2014).
- [37] L. D. Landau and E. M. Lifshitz, *Statistical Physics*, (Course of Theoretical Physics, Vol. 5, 3rd ed., revised and enlarged) (Pergamon Press, Oxford, 1980).
- [38] A. Mazeliauskas and D. Teaney, *Phys. Rev. C* **93**, 024913 (2016).

- [39] R. S. Bhalerao, J.-Y. Ollitrault, S. Pal, and D. Teaney, *Phys. Rev. Lett.* **114**, 152301 (2015).
- [40] L. Pang, Q. Wang, and X.-N. Wang, *Phys. Rev. C* **86**, 024911 (2012).
- [41] E. Shuryak and I. Zahed, *Phys. Rev. C* **88**, 044915 (2013).
- [42] F. Retiere and M. A. Lisa, *Phys. Rev. C* **70**, 044907 (2004).
- [43] S. Chatterjee *et al.*, *Adv. High Energy Phys.* **2015**, 349013 (2015).
- [44] B. I. Abelev (STAR Collaboration), *Phys. Rev. C* **79**, 034909 (2009).
- [45] B. Abelev (ALICE Collaboration), *Phys. Rev. C* **88**, 044910 (2013).
- [46] J. Cleymans, H. Oeschler, K. Redlich, and S. Wheaton, *Phys. Rev. C* **73**, 034905 (2006).
- [47] A. Andronic, P. Braun-Munzinger, and J. Stachel, *Phys. Lett. B* **673**, 142 (2009).
- [48] B. Abelev (ALICE Collaboration), *Eur. Phys. J. C* **74**, 3077 (2014).
- [49] S. S. Adler (PHENIX Collaboration), *Phys. Rev. C* **71**, 034908 (2005).
- [50] B. Alver (PHOBOS Collaboration), *Phys. Rev. C* **83**, 024913 (2011).